

# Validating the bright Gaia celestial reference frame with new VLBI astrometry of radio stars

J. Zhang<sup>1,2</sup>, B. Zhang<sup>1,\*</sup>, S. Xu<sup>3</sup>, and X. Mai<sup>1,2,4</sup>

<sup>1</sup> Shanghai Astronomical Observatory, Chinese Academy of Sciences, 80 Nandan Road, Shanghai 200030, People's Republic of China

<sup>2</sup> University of Chinese Academy of Sciences, No.19 (A) Yuquan Rd, Shijingshan, Beijing 100049, People's Republic of China

<sup>3</sup> Korea Astronomy and Space Science Institute, 776 Daedeok-daero, Yuseong-gu, Daejeon 34055, Republic of Korea

<sup>4</sup> University of Helsinki, P.O. Box 64, FI-00014, Finland

July 15, 2025

## ABSTRACT

**Aims.** There exist inconsistencies between the bright and faint Gaia Celestial Reference Frame 3 (Gaia-CRF3), which manifests as a systematic rotation and needs to be independently estimated then corrected in future data releases.

**Methods.** We collected 64 radio stars with very long baseline interferometry (VLBI) astrometry, of which 16 have new VLBI observations with reference epochs close to Gaia. We estimated the orientation and spin biases of the bright Gaia-CRF3 by comparing VLBI radio star astrometry with their Gaia DR3 counterparts. We also attempted to estimate orientation by utilizing the a priori magnitude-dependent spin parameters derived from Gaia's internal estimations.

**Results.** Our independent estimation of the orientation at  $G < 10.5$  is  $[-15 \pm 119, +330 \pm 139, +218 \pm 109] \mu\text{as}$  (J2016.0), and the spin  $([+21 \pm 18, +52 \pm 20, -7 \pm 20] \mu\text{as yr}^{-1})$  agrees with Gaia's internal estimation within a  $1\sigma$  range. The orientation-only estimation suggests that the orientation bias of the bright Gaia-CRF3 may also be magnitude-dependent.

**Key words.** astrometry – reference systems – proper motions

## 1. Introduction

The Gaia mission (Gaia Collaboration et al. 2016) provides precise astrometry for 1.8 billion sources in its latest data release, Gaia DR3 (Gaia Collaboration et al. 2023), and established its celestial reference frame, Gaia-CRF3 (Gaia Collaboration et al. 2022), based on an extragalactic source (quasar) sample of 1.6 million. However, most quasars are faint in the optical band, the  $G$ -band magnitude of which ranges from 13 to 21, without coverage of the bright end ( $G < 13$ ). This may result in potential inconsistency at the bright end. Unfortunately, evidence suggests that this inconsistency exists and manifests as a systematic rotation (orientation bias at reference epoch and spin with time) (Lindegren et al. 2018; Brandt 2018). The origin of this rotation may be astrometric instrument calibration limitations, such as window class effects (Lindegren 2020).

The rotation can be estimated internally within Gaia or through a comparison with the Hipparcos catalog (van Leeuwen 2007). For example, Cantat-Gaudin & Brandt (2021) estimated spin parameters with samples collected from known binaries and open clusters, and an ad hoc correction is applied in the astrometric solution of Gaia DR3 based on a comparison of proper motions with Hipparcos (Lindegren et al. 2021b).

It is necessary to validate the above estimations with independent external methods. For example, very long baseline interferometry (VLBI) astrometry of radio stars is a direct approach for the validation (Malkin 2016). Gaia-CRF3 is aligned to the International Celestial Reference Frame 3 (ICRF3, Charlot et al. 2020) using common quasars at the faint end. Al-

though there are still inconsistencies in a small number of common quasars (Charlot 2025), the overall alignment uncertainty is about  $7 \mu\text{as}$  (Gaia Collaboration et al. 2022). Since VLBI astrometry of radio stars is on an ICRF base, a comparison between VLBI and Gaia astrometry of radio stars can give an estimation of orientation and spin parameters between the bright and faint end of Gaia-CRF. There have been several related works, such as Lindegren (2020), Bobylev (2022), Lunz et al. (2023), Lunz et al. (2024), and Zhang et al. (2024), but the small sample size of available radio stars limits the reliability of their results.

In our previous studies, we observed 16 radio stars in total with the Very Long Baseline Array (VLBA), which significantly expanded the available radio star sample (Chen et al. 2023, Jiang et al. in prep., Zhang et al. in prep.). In this paper, we present a new CRF alignment result based on radio stars, integrating historical data with our new data. The data we use are introduced in Sect. 2. Sect. 3 describes the methods and results of the CRF alignment. We sum up in Sect. 4.

## 2. Data

### 2.1. VLBI data

The VLBI data used in this study consist of two parts: historical data and our new data. Lindegren (2020) collected 41 radio stars that have both VLBI parallaxes and proper motions and full astrometry in Gaia DR2. However, some of the data are old and the positions of their calibrators are out of date. Lunz et al. (2023) transferred these positions to the latest ICRF3, and provided new one-epoch VLBA observations of 32 radio stars (in which one is fainter than  $G = 13$ , and therefore not used in this study). We

\* Corresponding author; e-mail: zb@shao.ac.cn

included all these data in our dataset for this study. In [Chen et al. \(2023\)](#), Jiang et al. in prep., and Zhang et al. in prep., we provide VLBI astrometry of 2, 3, and 11 radio stars, respectively. These data include 15 stars with full five-parameter astrometry and 1 with two one-epoch observations, and are all included in our dataset. All historical and new VLBI data are listed in Appendix A, including 64 radio stars. Note that some stars have multiple data sources (e.g., we reobserved several “old” stars).

## 2.2. Gaia data

We collected Gaia counterparts of our VLBI samples, all of which have full five-parameter astrometry in Gaia DR3, and their  $G$  magnitudes range from 4.5 to 13. The parallax zero-point problem of Gaia DR3 may affect the usage of one-epoch VLBI data, so we corrected it using the recipe provided by [Lindegren et al. \(2021a\)](#), with coefficients given by [Ding et al. \(2024\)](#).

## 3. Estimation of the rotation between the bright Gaia-CRF3 and ICRF3

### 3.1. Solution of both orientation and spin parameters

We applied the CRF alignment solution method introduced in Sect. 2 of [Zhang et al. \(2024\)](#) to the radio star dataset. In simple terms, we assumed that there exists a time-dependent rotation between the bright Gaia-CRF3 and ICRF3, and that it can be described with a set of six parameters  $\mathbf{x} = [\varepsilon_X(T), \varepsilon_Y(T), \varepsilon_Z(T), \omega_X, \omega_Y, \omega_Z]'$ , of which the first three parameters describe an orientation bias at reference epoch  $T = J2016.0$ , while the last three parameters describe a spin at a constant angular velocity (or: the time derivative of orientation). This rotation can be estimated from the differences between VLBI and Gaia astrometry of the same sources. Because the rotation is on a small scale (hundreds of microarcseconds for orientation and tens of microarcseconds per year for spin), a linear approximation satisfies the need for accuracy, and we applied the least-square method to solve the parameters.

Not all radio stars are suitable for the CRF alignment solution, for different reasons, such as the intrinsic physical properties of the stars. For these stars, there may exist quite large differences between VLBI and Gaia astrometry, which will interfere with the estimation of CRF rotation. To eliminate these radio stars with high loss (outliers), we applied a similar iteration procedure to the one [Lindegren \(2020\)](#), [Lunz et al. \(2023\)](#), [Zhang et al. \(2024\)](#), and [Lunz et al. \(2024\)](#) used. The solution was first applied to the entire dataset ( $0 < G < 13$ ) including  $m = 64$  stars, then the star  $i$  ( $i = 1 \dots m$ ) with the highest loss ( $Q_i/v_i$ , normalized by the dimension of VLBI data) was rejected and the solution was applied again to the remaining stars. The iteration was repeated for  $k = 0, 1, \dots$  rejected stars. The evolutions of  $\max(Q_i/v_i)$ , reduced chi-square ( $\chi^2_{\text{red}}$ ), and estimated rotation parameters are shown in Figure 1.

In the initial rounds of iteration, due to the influence of outliers,  $\chi^2_{\text{red}}$  is very large and the rotation parameters also change drastically. As  $k$  increases,  $\chi^2_{\text{red}}$  and rotation parameters decrease and tend to be stable, and the  $\max Q_i/v_i$  drops below 30 when  $k = 19$ , at which time the maximum in the remaining samples is 26.18 (VY CMa). The rotation parameters also keep stable between  $k = 17$  and 21, so we adopted the result at  $k = 17$  for the solution, with a remaining accepted star number of  $l = 47$  and  $\chi^2_{\text{red}} = 5.346$ , as is shown in Table 1. Compared to the results of [Lunz et al. \(2024\)](#), the uncertainties of the parameters

are improved by roughly 50% and 30% in orientation and spin, respectively, benefitting from the additional VLBI data.

However, systematic inconsistencies do not only exist between magnitudes above and below  $G = 13$  in Gaia DR3. As is shown in Fig. 4 of [Cantat-Gaudin & Brandt \(2021\)](#) and Fig. 20 of [Lindegren et al. \(2021a\)](#), both proper motion and parallax biases are not stable between  $G = 10.5$  and 13. The magnitude dependency may explain why the result of solution  $0 < G < 13$  does not agree very well with that of [Lunz et al. \(2024\)](#), especially in orientation parameters. The new astrometry we added changes the magnitude distribution of the radio star sample, and due to the epochs being close to the Gaia reference epoch, the new data have a high weight in the orientation estimation, which has a great impact on the result.

Internal estimations of the relationships between CRF spin and  $G$  magnitude can be conducted by dividing binary and open cluster samples into multiple magnitude bins, but the number of VLBI radio star samples is too small to do so. Therefore, we tried to solve rotation parameters with a magnitude limit of  $G < 10.5$ , and the remaining star number is 50. A similar iteration was conducted (iteration shown in Appendix B, statistics shown in Appendix C), and we adopted the result at  $k = 13$  for the solution, with a remaining star number of  $l = 37$  and  $\chi^2_{\text{red}} = 5.627$ .

The results of solution  $0 < G < 10.5$  are also listed in Table 1 and agree well with [Cantat-Gaudin & Brandt \(2021\)](#): the spin parameters are within a  $1\sigma$  range of the internal estimation at  $G < 10.5$ . The agreement between internal and external estimations is quite satisfying and is strong proof of the existence of systematic rotation between the bright and faint (quasar-based) Gaia-CRF3 (which is precisely aligned with ICRF3).

### 3.2. Solution of orientation parameters only

We noticed that the discrepancies in orientation parameters between solution  $0 < G < 13$  and  $0 < G < 10.5$  are much beyond  $1\sigma$ , and so we conducted further investigations into it. It is necessary to fix spin parameters, then we can study orientation parameters independently. Since the spin parameters of solution  $G < 10.5$  agree well with [Cantat-Gaudin & Brandt \(2021\)](#), we tend to accept that their results are reliable. We therefore tried to solve orientation parameters with spin parameters from [Cantat-Gaudin & Brandt \(2021, Table 1\)](#) as a priori values. This approach has several advantages:

1. A priori values are given as a set of spin parameters for each of the 12 magnitude bins, which better reflects reality than using a set of magnitude-independent spin parameters;
2. Only three orientation parameters need to be solved in the solution, reducing the negative impact of the limited sample size;
3. Similar to (2), now we can try to solve for several magnitude bins to examine the relationship between CRF orientation and the  $G$  magnitude.

The mathematical form of the solution needs to be slightly modified; this is introduced in Appendix E. We solved for  $0 < G < 13$ ,  $0 < G < 10.5$ , and  $10.5 < G < 13$ , respectively. The sky distribution of the samples is shown in Appendix D, and the results are listed in Table 1. As is shown in Fig. 2, the results show that the orientation parameters change with  $G$  magnitude, which suggests that the orientation bias of the bright Gaia-CRF3 may also be magnitude-dependent. However, due to the limited sample size of each bin (especially  $10.5 < G < 13$ ), the uncertainties are relatively large. The results may also be biased by

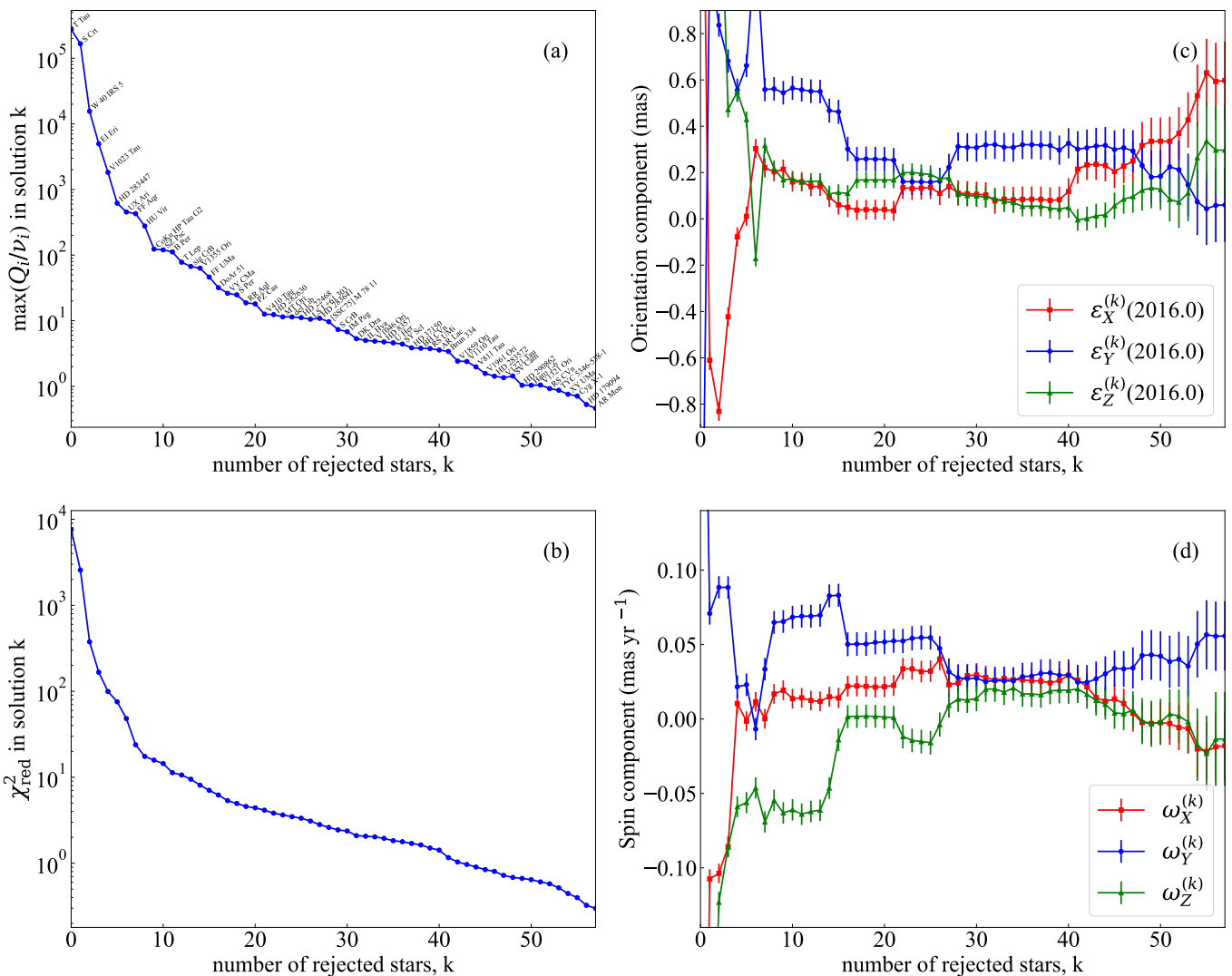


Fig. 1: Evolution of loss and rotation parameters with rejected star number,  $k$ , increasing in the full dataset ( $0 < G < 13$ ). (a) Max  $Q_i(\mathbf{x})$  in the solution (star names labeled). (b)  $\chi^2_{\text{red}}$  of the solution. (c) Estimated orientation parameters. (d) Estimated spin parameters. The error bars are formal uncertainties directly derived from the covariance matrix.

systematic offsets of some samples; for example, radio-optical offsets of the stars or position errors of calibrators. Therefore, additional VLBI astrometry of radio stars is essential to achieve more robust and conclusive results.

## 4. Summary

We have given an external estimation of the orientation and spin biases of the bright Gaia-CRF3 by comparing VLBI radio star astrometry and their Gaia DR3 counterparts. We collected all available VLBI astrometry for 64 radio stars, including historical and new observations, and found:

1. Our external estimation of spin parameters at  $G < 10.5$  ( $[+21 \pm 18, +52 \pm 20, -7 \pm 20] \mu\text{as yr}^{-1}$ ) agrees with Gaia's internal estimation (binaries and open clusters, [Cantat-Gaudin & Brandt 2021](#)) within a  $1\sigma$  range;
  2. Taking spin parameters from the internal estimation as a priori values, our estimation of the orientation parameters suggests that the orientation bias of the bright Gaia-CRF3 may also be magnitude-dependent.

External estimation with radio stars is now the only way to determine the orientation of the bright Gaia-CRF. Our analysis demonstrates that the orientation in the bright-end Gaia-CRF samples exhibits a possible magnitude dependency. While the present sample size of 11 stars in the range of  $10.5 < G < 13$  provides a foundational insight, it underscores the need for additional radio stars with VLBI astrometry. Drawing parallels from the Gaia parallax zero-point, which is known to vary with  $G$  magnitude, color, sky position, and other potential factors, we emphasize the importance of a more even sky distribution and covering different magnitudes uniformly in future observations. Such efforts are expected to not only refine uncertainties in parameter estimation but also enable optimized binning strategies and mitigate potential selection biases.

**Acknowledgements.** The Python code for CRF link is available at [Zhang \(2025\)](#). This work is supported by the National Natural Science Foundation of China (NSFC) under grant No. U2031212, the National Key R&D Program of China (No. 2024YFA1611500), and the Strategic Priority Research Program of the Chinese Academy of Sciences, Grant No. XDA0350205. This work has made use of data from the European Space Agency (ESA) mission Gaia (<https://www.cosmos.esa.int/gaia>), processed by the Gaia Data Processing and Analysis Consortium (DPAC, <https://www.cosmos.esa.int/web/gaia/dpac/consortium>). Funding

Table 1: Results of CRF alignment solution

Solution	$k$	$l$	Orientation at $T = \text{J2016.0}$ (mas)			Spin (mas yr $^{-1}$ )			$\chi^2_{\text{red}}$
			$\varepsilon_X(T)$	$\varepsilon_Y(T)$	$\varepsilon_Z(T)$	$\omega_X$	$\omega_Y$	$\omega_Z$	
$0 < G < 13$	17	47	+0.038 $\pm$ 0.043	+0.257 $\pm$ 0.053	+0.167 $\pm$ 0.036	+0.022 $\pm$ 0.007	+0.050 $\pm$ 0.008	+0.002 $\pm$ 0.008	5.346
			$\pm$ 0.099	$\pm$ 0.122	$\pm$ 0.082	$\pm$ 0.016	$\pm$ 0.018	$\pm$ 0.018	
$0 < G < 10.5$	13	37	-0.015 $\pm$ 0.050	+0.330 $\pm$ 0.059	+0.218 $\pm$ 0.046	+0.021 $\pm$ 0.007	+0.052 $\pm$ 0.008	-0.007 $\pm$ 0.009	5.627
			$\pm$ 0.119	$\pm$ 0.139	$\pm$ 0.109	$\pm$ 0.018	$\pm$ 0.020	$\pm$ 0.020	
$0 < G < 9$						+0.018 $\pm$ 0.005	+0.034 $\pm$ 0.005	-0.011 $\pm$ 0.006	
$9 < G < 9.5$						+0.014 $\pm$ 0.005	+0.031 $\pm$ 0.006	-0.019 $\pm$ 0.006	
$9.5 < G < 10$			spin-only, <a href="#">Cantat-Gaudin &amp; Brandt (2021)</a>			+0.013 $\pm$ 0.005	+0.031 $\pm$ 0.005	-0.012 $\pm$ 0.005	
$10 < G < 10.5$						+0.014 $\pm$ 0.004	+0.036 $\pm$ 0.004	-0.011 $\pm$ 0.004	
$0 < G < 13$	16	45	+0.117 $\pm$ 0.041	+0.448 $\pm$ 0.051	+0.170 $\pm$ 0.034				6.718
			$\pm$ 0.108	$\pm$ 0.132	$\pm$ 0.089				
$0 < G < 10.5$	13	34	+0.054 $\pm$ 0.048	+0.531 $\pm$ 0.056	+0.275 $\pm$ 0.043		orientation-only solution		6.221
			$\pm$ 0.119	$\pm$ 0.139	$\pm$ 0.108		adopting spin from <a href="#">Cantat-Gaudin &amp; Brandt (2021)</a>		
$10.5 < G < 13$	3	11	+0.189 $\pm$ 0.089	+0.098 $\pm$ 0.131	-0.025 $\pm$ 0.060				7.914
			$\pm$ 0.251	$\pm$ 0.369	$\pm$ 0.169				

**Notes.** The uncertainties in the second row of each solution are multiplied by  $\sqrt{\chi^2_{\text{red}}}$ . Correlation coefficients are listed in Appendix F.

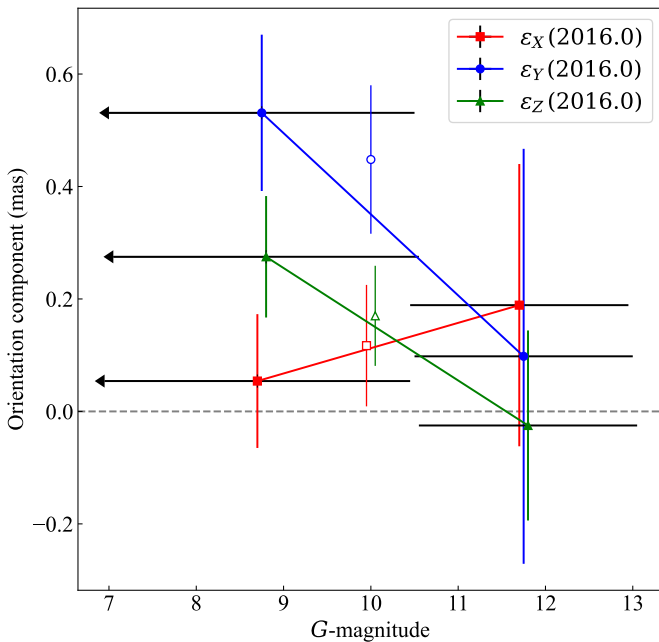


Fig. 2: Orientation-magnitude relationship of orientation-only solutions. Hollow markers denote the solution  $0 < G < 13$ . Markers are horizontally shifted by 0.05 to avoid error bars overlapping. Horizontal lines of markers represent their magnitude range.

for the DPAC has been provided by national institutions, in particular the institutions participating in the Gaia Multilateral Agreement. The Gaia services (<https://gaia.ari.uni-heidelberg.de/index.html>) provided by the Astronomisches Rechen-Institut (ARI) of the University of Heidelberg are used in Gaia data retrieval. The Python package for Gaia DR3 parallax zero-point correction developed by P. Ramos can be found at [https://gitlab.com/icc-ub/public/gaiadr3\\_zeropoint](https://gitlab.com/icc-ub/public/gaiadr3_zeropoint), and the coefficients used in this paper can be found at <https://github.com/yedings/Parallax-bias-correction-in-the-Galactic-plane>. This work has made use of the SIMBAD database, operated at CDS, Strasbourg, France (Wenger et al. 2000, <https://simbad.u-strasbg.fr/simbad/>). Python packages used in this work (in alphabetical order): Astropy (Astropy Collaboration et al. 2022), Matplotlib (Hunter 2007), Numpy (Harris et al. 2020), and Pandas (The pandas development Team 2024).

## References

- Asaki, Y., Deguchi, S., Imai, H., et al. 2010, ApJ, 721, 267
- Astropy Collaboration, Price-Whelan, A. M., Lim, P. L., et al. 2022, ApJ, 935, 167
- Bartel, N., Bietenholz, M. F., Lebach, D. E., et al. 2015, Classical and Quantum Gravity, 32, 224021
- Bobylev, V. V. 2022, Astronomy Letters, 48, 790
- Brandt, T. D. 2018, ApJS, 239, 31
- Cantat-Gaudin, T. & Brandt, T. D. 2021, A&A, 649, A124
- Charlot, P. 2025, in International VLBI Service for Geodesy and Astrometry 2024 General Meeting Proceedings, ed. D. Behrend, K. D. Baver, & K. L. Armstrong, 300
- Charlot, P., Jacobs, C. S., Gordon, D., et al. 2020, A&A, 644, A159
- Chen, W., Zhang, B., Zhang, J., et al. 2023, MNRAS, 524, 5357
- Ding, Y., Liao, S., Wu, Q., Qi, Z., & Tang, Z. 2024, A&A, 691, A81
- Gaia Collaboration, Klioner, S. A., Lindegren, L., et al. 2022, A&A, 667, A148
- Gaia Collaboration, Prusti, T., de Bruijne, J. H. J., et al. 2016, A&A, 595, A1
- Gaia Collaboration, Vallenari, A., Brown, A. G. A., et al. 2023, A&A, 674, A1
- Galli, P. A. B., Loinard, L., Ortiz-León, G. N., et al. 2018, ApJ, 859, 33
- Harris, C. R., Millman, K. J., van der Walt, S. J., et al. 2020, Nature, 585, 357
- Hunter, J. D. 2007, Computing in Science and Engineering, 9, 90
- Kounkel, M., Hartmann, L., Loinard, L., et al. 2017, ApJ, 834, 142
- Kusuno, K., Asaki, Y., Imai, H., & Oyama, T. 2013, ApJ, 774, 107
- Lestrade, J. F., Preston, R. A., Jones, D. L., et al. 1999, A&A, 344, 1014
- Lindegren, L. 2020, A&A, 633, A1
- Lindegren, L., Bastian, U., Biermann, M., et al. 2021a, A&A, 649, A4
- Lindegren, L., Hernández, J., Bombrun, A., et al. 2018, A&A, 616, A2
- Lindegren, L., Klioner, S. A., Hernández, J., et al. 2021b, A&A, 649, A2
- Loinard, L., Torres, R. M., Mioduszewski, A. J., et al. 2007, ApJ, 671, 546
- Lunz, S., Anderson, J. M., Xu, M. H., et al. 2024, A&A, 689, A134
- Lunz, S., Anderson, J. M., Xu, M. H., et al. 2023, A&A, 676, A11
- Malkin, Z. 2016, MNRAS, 461, 1937
- Melis, C., Reid, M. J., Mioduszewski, A. J., Stauffer, J. R., & Bower, G. C. 2014, Science, 345, 1029
- Miller-Jones, J. C. A., Sivakoff, G. R., Knigge, C., et al. 2013, Science, 340, 950
- Nakagawa, A., Omodaka, T., Handa, T., et al. 2014, PASJ, 66, 101
- Nakagawa, A., Tsushima, M., Ando, K., et al. 2008, PASJ, 60, 1013
- Nyu, D., Nakagawa, A., Matsui, M., et al. 2011, PASJ, 63, 63
- Ortiz-León, G. N., Dzib, S. A., Kounkel, M. A., et al. 2017a, ApJ, 834, 143
- Ortiz-León, G. N., Loinard, L., Kounkel, M. A., et al. 2017b, ApJ, 834, 141
- Peterson, W. M., Mutel, R. L., Lestrade, J. F., Güdel, M., & Goss, W. M. 2011, ApJ, 737, 104
- Reid, M. J., McClintock, J. E., Narayan, R., et al. 2011, ApJ, 742, 83
- The pandas development Team. 2024, pandas-dev/pandas: Pandas
- Torres, R. M., Loinard, L., Mioduszewski, A. J., et al. 2012, ApJ, 747, 18
- Torres, R. M., Loinard, L., Mioduszewski, A. J., & Rodríguez, L. F. 2007, ApJ, 671, 1813
- van Leeuwen, F. 2007, Hipparcos, the New Reduction of the Raw Data, Vol. 350
- Vlemmings, W. H. T. & van Langevelde, H. J. 2007, A&A, 472, 547
- Wenger, M., Ochsenbein, F., Egret, D., et al. 2000, A&AS, 143, 9
- Zhang, B., Reid, M. J., Menten, K. M., & Zheng, X. W. 2012, ApJ, 744, 23
- Zhang, J. 2025, FrdCHK/CRF\_link\_algorithm: First release
- Zhang, J., Zhang, B., Xu, S., et al. 2024, MNRAS, 529, 2062

## Appendix A: VLBI data used for CRF alignment

Table A.1: Five-parameter VLBI data used for CRF alignment

Star	Epoch	RA (h:m:s)	DEC (d:m:s)	$\sigma_{\alpha*}$ (mas)	$\sigma_{\delta}$ (mas)	$\varpi$ (mas)	$\mu_{\alpha*}$ (mas yr $^{-1}$ )	$\mu_{\delta}$ (mas yr $^{-1}$ )	Ref.
SY Scl	2006.828200	00:07:36.2468069	-25:29:40.028423	15.138	7.736	0.750±0.030	5.570±0.040	-7.320±0.120	1
HD 8357	2023.250000	01:22:56.9041707	+07:25:14.704379	0.351	0.738	22.638±0.366	93.885±0.223	230.683±0.483	2
S Per	2000.888400	02:22:51.7103447	+58:35:11.443414	8.678	9.040	0.413±0.017	-0.490±0.230	-1.190±0.200	3
LS I+61 303	1992.000000	02:40:31.6644017	+61:13:45.596676	0.291	0.573	0.260±0.610	0.967±0.260	-1.210±0.320	4
RZ Cas	2021.125966	02:48:55.5212829	+69:38:04.232909	0.238	0.234	15.274±0.093	2.965±0.318	37.543±0.185	5
UX Ari	1991.247100	03:26:35.3613614	+28:42:55.225562	0.444	0.495	19.370±0.390	41.617±0.186	-104.010±0.200	4
UX Ari	1999.986300	03:26:35.3838431	+28:42:54.275756	1.313	0.918	19.900±0.500	44.960±0.130	-102.330±0.090	6
HD 22468	1992.000000	03:36:47.3072102	+00:35:17.236072	0.406	0.401	33.880±0.470	-31.588±0.330	-161.690±0.310	4
V1271 Tau	2013.000000	03:43:48.3513936	+25:00:15.202980	0.110	0.171	7.418±0.025	19.860±0.050	-45.410±0.160	7
V811 Tau	2013.000000	03:45:21.2049588	+23:43:38.308879	0.118	0.198	7.223±0.057	19.470±0.110	-44.390±0.270	7
E1 Eri	2023.250000	04:09:40.9526282	-07:53:31.731358	0.229	0.374	17.894±0.146	36.433±0.097	111.925±0.109	2
HD 283447	1993.880900	04:14:12.9195008	+28:12:12.439088	0.585	0.895	6.740±0.250	0.423±0.291	-23.250±0.280	4
HD 283447	2006.970000	04:14:12.9224442	+28:12:12.170880	0.405	0.522	7.700±0.190	17.092±0.077	-24.030±0.053	8
V410 Tau	2015.760000	04:18:31.1187088	+28:27:15.760309	0.062	0.078	7.751±0.027	8.703±0.017	-24.985±0.020	9
V1023 Tau	2005.352500	04:18:47.0324242	+28:20:07.379058	0.054	0.244	7.530±0.030	4.300±0.050	-28.900±0.300	10
HD 283572	2005.352500	04:21:58.8520402	+28:18:06.371139	0.305	0.094	7.780±0.040	8.880±0.060	-26.600±0.100	10
HD 283572	2005.360000	04:21:58.8520428	+28:18:06.370962	0.073	0.079	7.841±0.057	9.023±0.061	-26.445±0.077	9
T Tau	2004.623100	04:21:59.4250676	+19:32:05.715231	0.145	0.633	6.820±0.030	4.020±0.030	-1.180±0.050	11
HD 283641	2015.950000	04:24:49.0581756	+26:43:10.128182	0.106	0.129	6.285±0.070	10.913±0.037	-16.772±0.044	9
V1110 Tau	2015.570000	04:34:39.2195622	+25:01:00.842376	0.230	0.322	11.881±0.149	-52.705±0.062	-11.321±0.066	9
HD 282630	2016.580000	04:55:36.9753264	+30:17:54.700203	0.188	0.228	7.061±0.125	3.897±0.113	-24.210±0.132	9
T Lep	2005.642700	05:04:50.8401301	-21:54:16.485482	30.255	13.266	3.060±0.040	14.600±0.500	-35.430±0.790	12
V1859 Ori	2023.250000	05:22:54.7948822	+08:58:04.463601	0.208	0.270	3.545±0.085	1.242±0.056	-9.372±0.034	2
V1961 Ori	2014.860000	05:34:27.3387259	-05:24:22.299151	0.141	0.255	2.533±0.027	-7.220±0.060	-0.990±0.080	13
Brun 334	2015.180000	05:34:39.7600265	-05:24:25.604141	0.138	0.275	2.591±0.046	-4.010±0.080	-1.170±0.070	13
V1321 Ori	2015.180000	05:35:04.3011976	-05:08:12.628523	0.190	0.409	2.509±0.044	0.060±0.200	6.950±0.160	13
MT Ori	2015.180000	05:35:17.9522494	-05:22:45.4355871	0.384	0.828	2.646±0.041	3.820±0.100	1.600±0.170	13
V1046 Ori	2015.200000	05:35:21.8682172	-04:29:39.000548	0.408	0.887	2.643±0.075	1.880±0.090	1.200±0.140	13
HD 37150	2015.190000	05:36:15.0289993	-05:38:52.516895	0.399	0.862	2.536±0.046	1.320±0.050	-0.560±0.120	13
TYC 5346-538-1	2015.200000	05:42:33.6768420	-08:07:15.182416	0.217	0.426	2.348±0.069	0.680±0.090	-0.510±0.250	13
HD 290862	2015.210000	05:46:43.3856400	+00:04:36.034276	0.790	1.132	2.197±0.545	0.350±0.270	0.830±0.830	13
[SSC75] M 78 11	2015.210000	05:46:45.3379210	+00:02:40.293196	0.342	0.574	2.547±0.034	0.010±0.100	-0.490±0.080	13
V1355 Ori	2023.250000	06:02:40.3788999	-00:51:36.953609	0.161	0.374	7.955±0.031	12.514±0.028	11.400±0.061	2
VY CMa	2006.530000	07:22:58.3259671	-25:46:03.062417	10.150	10.336	0.830±0.080	-2.210±0.060	2.290±0.300	14
XY UMa	2023.250000	09:09:55.8026472	+54:29:13.477129	0.399	0.662	14.729±0.571	-49.789±0.427	-182.889±0.328	2
FF UMa	2023.250000	09:33:46.4791651	+62:49:39.738521	0.128	0.130	8.470±0.098	-20.057±0.073	-22.157±0.072	2
DM UMa	2023.250000	10:55:43.4245688	+60:28:09.544893	0.184	0.213	5.473±0.075	-37.848±0.050	-7.598±0.054	2
SCrt	2005.798800	11:52:44.9697296	-07:35:48.086977	1.833	13.336	2.330±0.130	-3.170±0.220	-5.410±0.220	15
RS CVn	2023.250000	13:10:36.8122478	+35:56:06.0666804	0.097	0.181	7.488±0.104	-49.973±0.051	20.643±0.107	2
BH CVn	1993.108800	13:34:47.7594787	+37:10:56.760002	0.373	0.455	22.210±0.450	85.496±0.131	-9.220±0.160	4

Table A.1: continued.

Star	Epoch	RA (h:m:s)	DEC (d:m:s)	$\sigma_{\alpha*}$ (mas)	$\sigma_{\delta}$ (mas)	$\varpi$ (mas)	$\mu_{\alpha*}$ (mas yr $^{-1}$ )	$\mu_{\delta}$ (mas yr $^{-1}$ )	Ref.
S CrB	2000.00000	15:21:23.9560824	+31:22:02.573040	-	2.360±0.230	-9.060±0.230	-12.520±0.290	16	
RS UMi	2023.25000	15:50:49.4500275	+72:12:40.428941	0.127	2.187±0.014	3.340±0.017	-8.684±0.180	2	
sig CrB	1990.001400	16:14:41.0675052	+33:51:31.873993	0.104	43.930±0.100	-267.048±0.037	-86.660±0.050	4	
U Her	2000.00000	16:25:47.4716736	+18:53:32.855640	-	3.740±0.610	-14.980±0.290	-9.230±0.320	16	
Haro 1-6	2007.990000	16:26:03.0160198	-24:23:36.405235	0.596	0.856	7.385±0.234	-19.630±0.190	-26.920±0.130	17
DoAr 51	2014.750000	16:32:11.7909539	-24:40:21.962916	0.534	0.836	6.983±0.050	-4.800±0.080	-23.110±0.110	17
W 40 IRS 5	2014.950000	18:31:14.8227619	-02:03:50.157308	0.156	0.291	2.302±0.063	0.186±0.053	-6.726±0.121	18
HD 179094	2021.125743	19:08:25.5551833	+52:25:31.480133	1.461	0.998	14.300±0.338	-102.158±2.449	-55.217±0.570	5
RR Aql	2000.000000	19:57:36.0597288	-01:53:11.338656	-	1.580±0.400	-25.110±0.740	-49.820±0.540	16	
Cyg X-1	1991.249800	19:58:21.6784714	+35:12:05.840028	0.308	0.368	0.730±0.300	-3.787±0.172	-6.250±0.210	4
Cyg X-1	2009.570000	19:58:21.6727548	+35:12:05.725022	0.500	0.500	0.547±0.041	-3.700±0.080	-6.420±0.140	19
HD 199178	1993.793300	20:53:53.6368109	+44:23:11.085234	0.332	0.397	8.590±0.330	26.595±0.407	-1.240±0.430	4
HD 199178	2020.895230	20:53:53.7035929	+44:23:11.062287	0.361	0.376	8.953±0.093	26.381±0.225	-0.876±0.177	20
SS Cyg	2011.566100	21:42:42.9230791	+43:35:10.253553	0.216	0.215	8.800±0.120	112.420±0.070	33.380±0.070	21
FF Aqr	2023.250000	22:00:36.4739751	-02:44:27.109979	0.126	0.212	4.564±0.072	32.774±0.043	-11.826±0.061	2
AR Lac	1992.435300	22:08:40.8558984	+45:44:31.751477	0.274	0.361	23.970±0.370	-52.080±0.126	47.030±0.190	4
AR Lac	2020.895340	22:08:40.7137036	+45:44:33.089029	0.161	0.126	23.529±0.130	-51.884±0.265	46.830±0.224	20
IM Peg	1992.917200	22:53:02.2762503	+16:50:28.492233	0.394	0.428	10.280±0.620	-20.587±0.459	-27.530±0.400	4
IM Peg	2005.086900	22:53:02.2586161	+16:50:28.159982	0.434	0.426	10.370±0.074	-20.833±0.090	-27.267±0.095	22
SZ Psc	2021.125933	23:13:23.8098299	+02:40:32.164513	0.650	0.935	10.134±0.243	13.158±0.843	26.790±0.235	5
PZ Cas	2006.299800	23:44:03.2815716	+61:47:22.187580	3.013	3.086	0.356±0.026	-3.700±0.200	-2.000±0.300	23

$\sigma_{\alpha*}$  and  $\sigma_{\delta}$  denote position errors in RA·cos(DEC) and DEC directions, respectively. Positional data without uncertainties ("") were not used in the solutions.

References: (1) [Nyú et al. \(2011\)](#); (2) [Zhang et al. in prep.](#); (3) [Asaki et al. \(2010\)](#); (4) [Lestrade et al. \(1999\)](#); (5) [Jiang et al. in prep.](#); (6) [Peterson et al. \(2011\)](#); (7) [Melis et al. \(2014\)](#); (8) [Torres et al. \(2012\)](#); (9) [Galli et al. \(2018\)](#); (10) [Torres et al. \(2007\)](#); (11) [Loinard et al. \(2014\)](#); (12) [Nakagawa et al. \(2007\)](#); (13) [Kounkel et al. \(2017\)](#); (14) [Zhang et al. \(2012\)](#); (15) [Nakagawa et al. \(2008\)](#); (16) [Vlemmings & van Langevelde \(2007\)](#); (17) [Ortiz-León et al. \(2017a\)](#); (18) [Ortiz-León et al. \(2017b\)](#); (19) [Reid et al. \(2011\)](#); (20) [Chen et al. \(2023\)](#); (21) [Miller-Jones et al. \(2013\)](#); (22) [Bartel et al. \(2015\)](#); (23) [Kusuno et al. \(2013\)](#).

Table A.2: One-epoch VLBI data used for CRF alignment

Star	Epoch	RA (h:m:s)	DEC (d:m:s)	$\sigma_{\alpha^*}$ (mas)	$\sigma_{\delta}$ (mas)	Ref.
UV Psc	2020.015060	01:16:55.2328601	+06:48:42.545459	0.286	0.700	1
HD 8357	2020.015070	01:22:56.8823023	+07:25:13.949756	0.283	0.694	1
LS I +61 303	2020.015200	02:40:31.6633188	+61:13:45.588648	0.315	0.701	1
RZ Cas	2020.015200	02:48:55.5183194	+69:38:04.194762	0.315	0.714	1
UX Ari	2020.015420	03:26:35.4456180	+28:42:52.171571	0.429	0.825	1
UX Ari	2020.015420	03:26:35.4455928	+28:42:52.170397	0.297	0.700	1
UX Ari	2020.015420	03:26:35.4455030	+28:42:52.171276	0.431	0.830	1
UX Ari	2020.015420	03:26:35.4454778	+28:42:52.170160	0.299	0.705	1
HD 22468	2020.015450	03:36:47.2457954	+00:35:12.688282	0.282	0.692	1
HD 283447	2020.015440	04:14:12.9344146	+28:12:11.807694	0.376	0.829	1
HD 283447	2020.015440	04:14:12.9344304	+28:12:11.809246	0.291	0.713	1
HD 283447	2020.015440	04:14:12.9346284	+28:12:11.809616	0.375	0.828	1
HD 283447	2020.015440	04:14:12.9346440	+28:12:11.811280	0.291	0.713	1
B Per	2020.015440	04:18:14.7095050	+50:17:42.686621	0.284	0.695	1
V410 Tau	2020.015460	04:18:31.1212018	+28:27:15.653570	0.287	0.703	1
HD 283572	2020.015470	04:21:58.8615370	+28:18:05.984222	0.284	0.695	1
T Tau	2020.015480	04:21:59.4376870	+19:32:05.551793	0.306	0.739	1
CoKu HP Tau G2	2020.015490	04:35:54.1727731	+22:54:13.186156	0.303	0.724	1
CoKu HP Tau G2	2020.015490	04:35:54.1728058	+22:54:13.186037	0.304	0.722	1
Brun 334	2020.015600	05:34:39.7587494	-05:24:25.609900	0.307	0.739	1
TYC 5346-538-1	2020.015610	05:42:33.6769745	-08:07:15.184528	0.337	0.788	1
SV Cam	2020.014610	06:41:19.5133901	+82:15:59.418299	0.283	0.695	1
AR Mon	2021.678721	07:20:48.4647784	-05:15:35.943515	0.109	0.253	2
AR Mon	2021.804318	07:20:48.4648528	-05:15:35.945308	0.075	0.164	2
54 Cam	2020.013580	08:02:35.6931432	+57:16:23.871857	0.300	0.700	1
IL Hya	2020.013480	09:24:48.9564576	-23:49:35.361127	0.302	0.740	1
HU Vir	2020.013710	12:13:20.6754857	-09:04:46.858105	0.306	0.740	1
DK Dra	2020.013620	12:15:41.4523546	+72:33:03.809124	0.308	0.702	1
RS CVn	2020.013700	13:10:36.8261232	+35:56:05.997422	0.283	0.694	1
BH CVn	2020.013700	13:34:47.9537587	+37:10:56.490899	0.319	0.726	1
BH CVn	2020.013700	13:34:47.9537057	+37:10:56.489448	0.318	0.737	1
del Lib	2020.014050	15:00:58.2632962	-08:31:08.335088	0.312	0.702	1
del Lib	2020.014050	15:00:58.2632419	-08:31:08.333656	0.350	0.827	1
sig CrB	2020.014160	16:14:40.4246654	+33:51:29.234981	0.282	0.691	1
Haro 1-6	2020.014290	16:26:02.9989615	-24:23:36.731260	0.319	0.789	1
DoAr 51	2020.014290	16:32:11.7895704	-24:40:22.082106	0.322	0.803	1
DoAr 51	2020.014290	16:32:11.7892778	-24:40:22.087733	0.324	0.808	1
HD 199178	2020.014520	20:53:53.7011153	+44:23:11.055530	0.394	0.753	1
SS Cyg	2020.014510	21:42:43.0100261	+43:35:10.528408	0.305	0.714	1
AR Lac	2020.014600	22:08:40.7168030	+45:44:33.030622	0.297	0.701	1
AR Lac	2020.014600	22:08:40.7167838	+45:44:33.030877	0.282	0.692	1
IM Peg	2020.014690	22:53:02.2364210	+16:50:27.746012	0.282	0.692	1
SZ Psc	2020.014750	23:13:23.8079419	+02:40:32.129994	0.471	1.106	1
SZ Psc	2020.014750	23:13:23.8079614	+02:40:32.130487	0.283	0.692	1

**Notes.** References: (1) [Lunz et al. \(2023\)](#); (2) Zhang et al., in prep.

## Appendix B: Iteration of solution $0 < G < 10.5$

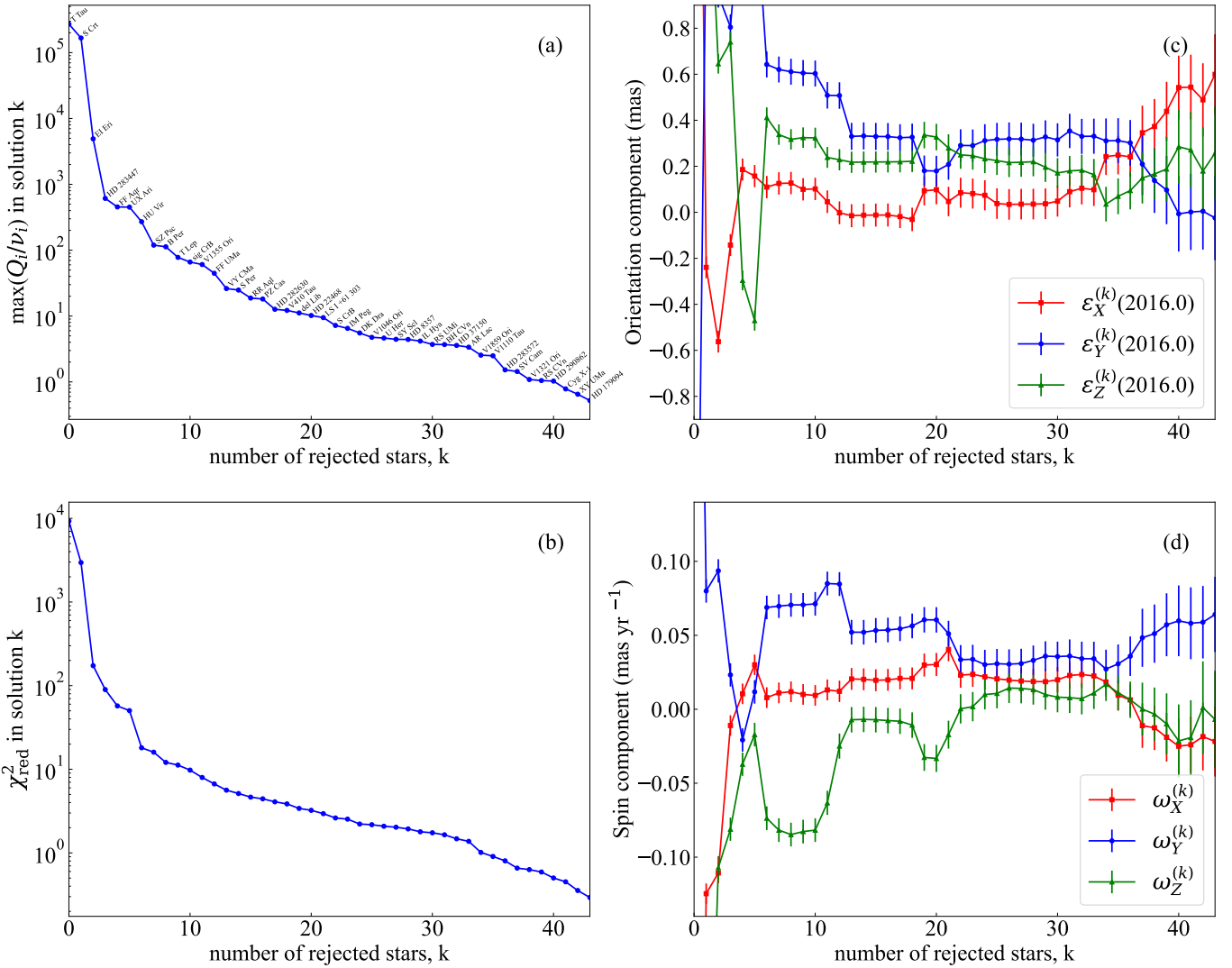


Fig. B.1: The evolution of loss and CRF link parameters with rejected star number  $k$  grows on the dataset  $0 < G < 10.5$ .

## Appendix C: Statistics of solution $0 < G < 10.5$

Table C.1: Statistics of solution  $0 < G < 10.5$  for each star

Star	$\nu$	$Q_i/\nu_i$	$E_i$ (mas $^{-2}$ )	$\Omega_i$ (mas $^{-2}\text{yr}^2$ )
SY Scl	5	4.65	0.0	93.8
S Per	5	24.82	0.0	43.7
LS I +61 303	7	11.78	22.2	5082.8
HD 22468	7	11.59	20.3	1435.6
V410 Tau	7	12.05	412.4	2725.2
HD 283572	12	1.54	73.8	4719.7
V1110 Tau	5	3.36	28.3	446.5
HD 282630	5	12.62	47.2	147.0
V1321 Ori	5	0.70	33.6	86.1
V1046 Ori	5	4.53	7.2	136.4
HD 37150	5	3.46	7.5	261.1
HD 290862	5	0.97	2.4	16.2
VY CMa	5	26.17	0.0	14.9
BH CVn	9	3.49	27.5	868.6
S CrB	3	7.19	0.0	27.4
U Her	3	4.70	0.0	20.6
RR Aql	3	18.76	0.0	5.1
Cyg X-1	10	1.60	13.4	4747.5
HD 199178	12	0.96	36.0	4232.6
AR Lac	14	3.08	153.7	3794.5
IM Peg	12	6.25	23.2	505.1
PZ Cas	5	18.14	0.2	53.3
UV Psc	2	0.17	12.9	207.4
HD 8357	7	5.14	13.3	460.0
RZ Cas	7	1.45	39.9	968.3
SV Cam	2	0.60	13.8	222.2
54 Cam	2	0.40	12.3	197.4
IL Hya	2	4.24	11.4	183.0
DK Dra	2	6.79	11.3	181.9
RS CVn	7	0.47	99.4	5050.1
del Lib	4	11.06	1.0	16.3
V1859 Ori	5	3.47	32.2	2591.0
AR Mon	4	0.47	57.2	1898.8
XY UMa	5	0.59	41.3	1113.0
DM UMa	5	0.93	40.6	3097.9
RS UMi	5	3.74	49.4	5551.0
HD 179094	5	0.51	1.3	36.1

**Notes.**  $\nu$  is the total VLBI data dimension of each star, e.g., 5 for five-parameter measurement and 2 for one-epoch measurement.  $Q_i/\nu_i$  is the normalized loss.  $E_i$  and  $\Omega_i$  are weights (amounts of information contributed) in orientation and spin respectively. Only accepted stars are listed in this table.

## Appendix D: Radio star sky distribution

The sky distribution of the radio stars is shown in Fig. D.1. The whole sample lacks stars in the southern sky ( $< -30^\circ$ ). The number of stars between  $G = 9$  and  $13$  is small and the stars are unevenly distributed, especially concentrated near the galactic plane, which may cause selection biases. A larger number of more evenly distributed available radio stars will help improve our results and reduce the impact of potential selection biases.

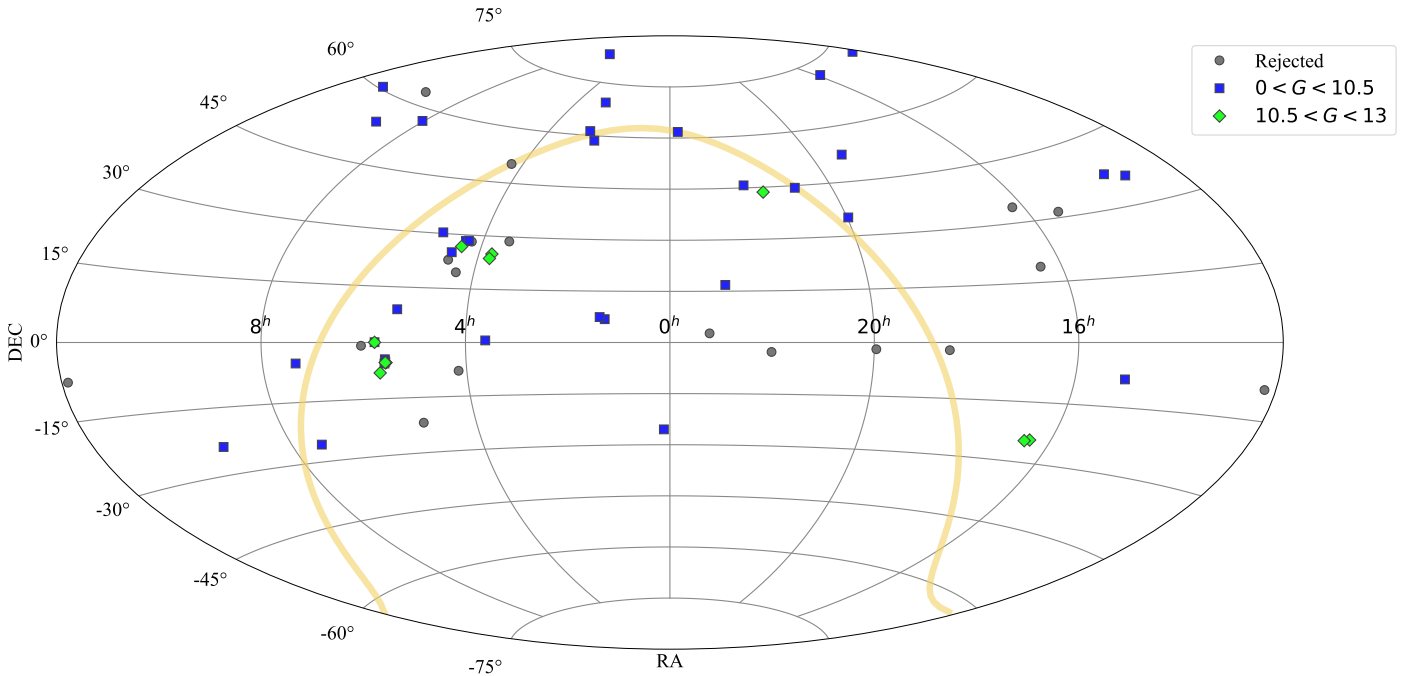


Fig. D.1: The sky distribution (Aitoff projection in equatorial coordinates) of the radio stars used in this study. The blue squares and green diamonds denote samples used in solution  $0 < G < 10.5$  and  $10.5 < G < 13$ , respectively. The rejected stars are plotted as grey dots. The Galactic Equator is plotted in yellow.

## Appendix E: Mathematics for orientation-only solution

The solution is based on Sect. 2 of Zhang et al. (2024), and the modifications needed for the orientation-only solution are as follows:

Proper motions of Gaia data  $\boldsymbol{\mu} = [\mu_{\alpha*}, \mu_{\delta}]'$  need to be corrected with the a priori spin parameter  $\boldsymbol{\omega} = [\omega_X, \omega_Y, \omega_Z]'$  before the solution

$$\boldsymbol{\mu}_{\text{corrected}} = \boldsymbol{\mu} - \mathbf{L}\boldsymbol{\omega}, \quad (\text{E.1})$$

where

$$\mathbf{L} = \begin{bmatrix} c\alpha_i s\delta_i & s\alpha_i s\delta_i & -c\delta_i \\ -s\alpha_i & c\alpha_i & 0 \end{bmatrix}; \quad (\text{E.2})$$

The parameters to be estimated is changed to  $\boldsymbol{x} = [\varepsilon_X(T), \varepsilon_Y(T), \varepsilon_Z(T)]'$ ;

Because of the shape of  $\boldsymbol{x}$  is changed from  $6 \times 1$  to  $3 \times 1$ , the coefficient matrix  $\mathbf{K}_i$  also needs to be changed to

$$\mathbf{K}_i = \begin{bmatrix} c\alpha_i s\delta_i & s\alpha_i s\delta_i & -c\delta_i \\ -s\alpha_i & c\alpha_i & 0 \\ 0 & 0 & 0 \\ 0 & 0 & 0 \\ 0 & 0 & 0 \end{bmatrix} \quad (\text{E.3})$$

to match the shape of  $\boldsymbol{x}$ .

## Appendix F: Solution correlation coefficient matrices

Solution  $0 < G < 13$

$$\text{corr}[\varepsilon_X(T), \varepsilon_Y(T), \varepsilon_Z(T), \omega_X, \omega_Y, \omega_Z] =$$

$$\begin{bmatrix} +1.000 & +0.191 & +0.204 & -0.102 & -0.120 & -0.206 \\ \dots & +1.000 & +0.277 & -0.139 & -0.214 & -0.105 \\ \dots & \dots & +1.000 & -0.177 & -0.090 & -0.154 \\ \dots & \dots & \dots & +1.000 & -0.032 & +0.099 \\ \dots & \dots & \dots & \dots & +1.000 & -0.021 \\ \dots & \dots & \dots & \dots & \dots & +1.000 \end{bmatrix} \quad (\text{F.1})$$

Solution  $0 < G < 10.5$

$$\text{corr}[\varepsilon_X(T), \varepsilon_Y(T), \varepsilon_Z(T), \omega_X, \omega_Y, \omega_Z] =$$

$$\begin{bmatrix} +1.000 & +0.134 & +0.192 & -0.166 & -0.100 & -0.237 \\ \dots & +1.000 & +0.255 & -0.132 & -0.279 & -0.091 \\ \dots & \dots & +1.000 & -0.213 & -0.068 & -0.280 \\ \dots & \dots & \dots & +1.000 & -0.043 & +0.120 \\ \dots & \dots & \dots & \dots & +1.000 & -0.043 \\ \dots & \dots & \dots & \dots & \dots & +1.000 \end{bmatrix} \quad (\text{F.2})$$

Orientation-only solution  $0 < G < 13$

$$\text{corr}[\varepsilon_X(T), \varepsilon_Y(T), \varepsilon_Z(T)] = \begin{bmatrix} +1.000 & +0.142 & +0.158 \\ \dots & +1.000 & +0.239 \\ \dots & \dots & +1.000 \end{bmatrix} \quad (\text{F.3})$$

Orientation-only solution  $0 < G < 10.5$

$$\text{corr}[\varepsilon_X(T), \varepsilon_Y(T), \varepsilon_Z(T)] = \begin{bmatrix} +1.000 & +0.069 & +0.102 \\ \dots & +1.000 & +0.206 \\ \dots & \dots & +1.000 \end{bmatrix} \quad (\text{F.4})$$

Orientation-only solution  $10.5 < G < 13$

$$\text{corr}[\varepsilon_X(T), \varepsilon_Y(T), \varepsilon_Z(T)] = \begin{bmatrix} +1.000 & +0.414 & +0.345 \\ \dots & +1.000 & +0.397 \\ \dots & \dots & +1.000 \end{bmatrix} \quad (\text{F.5})$$